Catalysis Science & Technology

ROYAL SOCIETY OF CHEMISTRY

PAPER

View Article Online
View Journal | View Issue

Cite this: *Catal. Sci. Technol.*, 2021, 11, 4280

The relevance of Lewis acid sites on the gas phase reaction of levulinic acid into ethyl valerate using CoSBA-*x*Al bifunctional catalysts†

M. Muñoz-Olasagasti,[a] M. López Granados, [a] C. P. Jiménez-Gómez,[b] J. A. Cecilia, [b] P. Maireles-Torres, [b] J. A. Dumesic [c] and R. Mariscal [*a]

Received 29th January 2021,
Accepted 27th April 2021

DOI: 10.1039/d1cy00166c

rsc.li/catalysis

A series of Co supported on Al-modified SBA-15 catalysts has been studied in the gas phase direct transformation of levulinic acid (LA) into ethyl valerate (EV) using a continuous fixed-bed reactor and ethanol as solvent. It was observed that once the intermediate product gamma-valerolactone (GVL) has been formed, the presence of aluminum is required for the selective transformation to EV. Three Lewis acid sites (LAS) are identified (from highest to lowest acid strength): aluminum ions in tetrahedral and octahedral coordination and Co^{2+} sites. The intrinsic activity of these LAS for the key reaction, the GVL ring opening, decreases with the strength of these acid sites, but so does the undesirable formation of coke, also catalyzed by these centers. The best catalyst was that with the highest Al content, CoSBA-2.5Al, that reached an EV yield of up to 70%. This result is associated with the presence of LAS attributed to the presence of Co^{2+} surface species that, although having low intrinsic activity in the selective GVL ring-opening reaction, are highly concentrated in this sample and also possess less activity in the undesirable and deactivating formation of coke. These Co^{2+} LAS have been stabilized by incorporation of aluminum into the support, modifying the reducibility and dispersion of cobalt species. Additionally, the lower proportion of metallic Co species decreases the hydrogenating capacity of this catalyst. This decrease is a positive result because it prevents GVL hydrogenation to undesired products. This catalyst also showed promising stability in a 140 h on-stream run.

1. Introduction

Levulinic acid (LA) is one of the main derivatives of biomass and constitutes a platform molecule due to the enormous number of chemicals and biofuels that can be obtained from it.[1,2] Because of the variety of possible reactions with LA and the wide range of valuable products, the hydrogenation of LA has been given an increasing amount of attention in recent years. Among these possibilities, valeric acid and its derived esters were originally proposed as valeric biofuels by Lange *et al.*[3] since they are fully compatible with current transportation fuels.

The catalytic transformation of LA to valerate esters using an alcohol as solvent goes through several tandem reactions and intermediates. Recently Yu *et al.*[4] have published an excellent review on the mechanism and heterogeneous catalytic systems active in this reaction. The formation of valerate esters requires the following consecutive steps: (1) hydrocyclization of LA to gamma-valerolactone (GVL) using hydrogenating and acid sites; (2) a ring-opening reaction on acid sites where GVL leads to the formation of pentenoate ester isomers; and (3) subsequent reduction to obtain the valerate esters. If this latter reaction is conducted in water, the main product of the reaction is valeric acid (VA), which later requires an esterification with alcohol in a second reactor. In recent years, the challenge of integrating these sequential reactions into a one-pot process and a bifunctional catalyst has been an area of interest. It is well agreed that the cascade transformation of LA to EV requires the presence of metal centers with a reducing capacity and active acid sites.

Among the bifunctional catalysts that lead to the highly efficient production of VA or its esters from LA are noble metals supported on acidic oxides. Some of the more remarkable bifunctional catalysts under batch experiments

[a] *Group of Sustainable Energy and Chemistry (EQS), Institute of Catalysis and Petrochemistry (ICP-CSIC), C/Marie Curie 2, Campus de Cantoblanco, 28049 Madrid, Spain. E-mail: r.mariscal@icp.csic.es*
[b] *Departamento de Química Inorgánica, Cristalografía y Mineralogía (Unidad Asociada al ICP-CSIC), Facultad de Ciencias, Universidad de Málaga, Campus de Teatinos, 29071 Málaga, Spain*
[c] *Department of Chemical and Biological Engineering, University of Wisconsin–Madison, Madison, WI 53706, USA*

† Electronic supplementary information (ESI) available. See DOI: 10.1039/d1cy00166c

are the following: Pt/HMFI catalyst,[5] with which 99% yield to VA was reached in a solvent-free reaction due to a cooperative mechanism of Pt and the Brønsted acid sites (BAS). Pt/HZSM-5 catalyst, which was prepared after five atomic layer deposition (ALD) cycles, was considered a highly active bifunctional catalyst with a satisfactory stability for the reaction processes and an excellent VA yield of 91.4% in aqueous solution.[6] Ru/HZSM-5 also gave a high VA yield of 91.3% in dioxane after 10 h.[7] Pan *et al.*[8] reported the effects of different supports and acidity levels on the hydrogenation of LA to valerate esters on Ru-based catalysts. A 94% yield of ethyl valerate and valeric acid (EV + VA) was achieved over the Ru/SBA-SO_3H catalyst using ethanol as solvent. The loading of catalysts was high, 43 wt% (referred to LA), and the catalyst was mainly deactivated by leaching of sulphonic sites. Pd/ZSM-5 also demonstrated an excellent performance, with high VA and EV yields (92%) after an 8 h reaction using ethanol as solvent.[9] Recently, it has also been reported that the metal selected can modulate the selectivity of LA into GVL or valeric biofuels using 1,4 dioxane as solvent. Thus, Ru/HZSM-5 catalysts exhibit a high yield (85.7%) of valeric biofuels, whereas Ni/HZSM-5 catalysts achieve a GVL yield of 93.1% with negligible formation of valeric acid or esters. It is found that the introduction of Ru into HZSM-5 would increase the number of strong acidic sites and enhance the ring opening of the GVL intermediate.[10] Many of these studies have been conducted at moderate temperatures and under H_2 pressure (473–523 K and 1–4 MPa H_2) together with an autogenous ethanol pressure under liquid phase conditions in a batch reactor.

The former noble metal-based catalysts are expensive and commonly suffer from deactivation by coke formation and deposition. Consequently, alternative catalysts based on low-cost non-noble metals that are resistant to deactivation are required. The latter implies the study of the stability in long-term experiments in a fixed bed continuous flow reactor. Co catalysts have shown activity in cascade reactions involved in the transformation of LA to EV. In this way, the Co/SBA-15 system has demonstrated excellent behavior under mild conditions. Specifically, GVL yields up to 78% were obtained at 423 K with 5.0 MPa H_2 and 2 h in a batch reactor.[11] Additionally, Sun *et al.*[12] reported a 97% yield of VA + EV in a batch reactor at 513 K with 3.0 MPa H_2 after 3 h of reaction using catalysts based on cobalt nanoparticles embedded in HZSM-5. Slow deactivation of the best catalyst was observed in a fixed-bed reactor under continuous conditions. The activity was entirely restored after regeneration *via* calcination followed by reduction of the catalysts, suggesting that the cause of deactivation was the deposition of coke formed in the surface acid sites. A non-noble metal catalyst based on Nb–Cu/Zr-doped porous silica (ZPS) catalyst has been recently described.[13] Under mild reaction conditions, 423 K and 3 MPa H_2 for 4 h in aqueous medium, a VA yield of 99.8% was reached. The Lewis acid sites of ZPS enhanced the adsorption of LA on the catalyst surface, and both the Lewis and Brønsted acidity associated with Nb_2O_5 and the metallic Cu^0 sites promoted catalysis of the tandem reaction. Nb_2O_5 avoids metal leaching and coke formation, which are serious issues in liquid phase reaction conditions. In summary, the hydrogenating function has been extensively studied, especially the nature of the supported metal. The reducing function of the bifunctional catalysts is required in two steps: the hydrogenation of LA to GVL and the reduction of ethyl pentenoate isomers into EV. Both reactions are not considerably challenging under these reaction conditions.

The role of the acid function has also been worthy of numerous studies in liquid and vapor phase systems. Even more, it has been reported that the rate-determining step of the reaction is the ring opening of the GVL driven by acid sites.[14] In the aforementioned studies, the acid function is mainly based on HZSM5 or SBA-15 functionalized by SO_3H groups, where strong BAS have been described as those with the highest intrinsic activity for the GVL ring opening. Sun *et al.*[15] studied the acidity regulation on the Ni/HZSM-5 catalyst by increasing the potassium content. Potassium decreases the acid strength together with an adjustment of the Brønsted/Lewis centers ratio in the flow reactor. More recently, Zhou *et al.*[16] have reported for the first time that strong Lewis acid sites (LAS) are also active for the ring opening of GVL. These authors have described a dual catalyst of Pd/C and $Hf(OTf)_4$ in a solution in *n*-octane. Under a relatively low temperature of 423 K and 5.0 MPa H_2, 92% VA selectivity at almost complete LA conversion was obtained.

In a different non-noble metal approach and using GVL as a substrate, the key intermediate in our cascade reaction, Ravasio *et al.*[17] have studied GVL transformation with a catalyst based in a non-noble metal supported on amorphous weakly acidic material, specifically Cu–SiZr systems. Using pentanol as the solvent, pentyl valerate can be obtained in one pot with GVL conversions of 90% and selectivity up to 83%. Liu *et al.*[18] have described a highly dispersed Cu/ZrO_2 catalyst due to a strong interaction between CuO and ZrO_2 in the precursor could lead to enhanced Cu dispersion and the formation of Cu^+ active centers. This catalyst presents low acidity and exhibited 85.4% conversion of GVL and 98% selectivity for pentyl valerate at 503 K and 1.5 MPa H_2 pressure. The success of these catalytic systems based on weakly acidic oxides opens an exciting alternative to noble metal–zeolite catalysts because they demonstrated that weak LAS are active in the GVL ring-opening reaction. Moreover, the weaker acid strength of these systems can prevent the deactivation of the catalyst by fouling with coke, which may prolong the practical life of the catalyst. A trade-off in the support acidity properties should be necessary to develop an efficient and stable bifunctional catalyst.

However, despite these efforts, a study for the direct reaction of LA to give EV with a bifunctional catalyst without strong BAS or LAS has not yet been conducted. The support oxide usually provides the acid function. Our approach to conduct such study has been to prepare a series of catalysts based on Co supported on Al-modified SBA-15 supports. The

Co concentration (metal hydrogenation function) was kept constant, whereas the Al content in the support SBA-15 was varied to change the nature, strength and concentration of the acid sites. The investigation presented here allows us to demonstrate that both Al^{3+}- and Co^{2+}-based LAS are capable of conducting the key acid-catalyzed reactions. Especially relevant are the latter, those defined by Co^{2+} sites stabilized by the incorporated Al oxide. Their relative weak strength, capable of performing the GVL ring-opening reaction, does not catalyze the formation of coke-like deposits that may prevent the deactivation by fouling.

2. Experimental procedure

2.1. Preparation of the CoSBA-*x*Al bifunctional catalysts

The synthesis of acid catalytic supports was conducted in two stages. First, SBA-15 mesoporous silicate was prepared following the method described by Gómez-Cazalilla *et al.*[19] 25 g of Pluronic was incorporated in 1 L of a 0.4 M sulfuric acid solution, and this mixture was gently stirred for one day at room temperature. Then, 1 g of sodium hydroxide was added along with a sodium silicate solution (66.4 mL of sodium silicate + 920 mL of distilled water), which was added dropwise under moderate agitation at room temperature. The resulting mixture (gel appearance) was stirred for five days at room temperature. The solid was recovered *via* vacuum filtration and washed several times with distilled water. Subsequently, it was dried in an oven at 353 K for 12 h and was finally calcined at 823 K for 6 h at a heating rate of 2 K min^{-1}. Second, to provide acidity over the catalyst support, aluminum was incorporated into SBA-15. The procedure was conducted by mixing different volumes of a 1.2 M $AlCl_3{\cdot}6H_2O$ aqueous solution with tetramethylammonium hydroxide (TMAOH, 25 wt%), keeping a TMAOH/Al ratio = 2.5 for all preparations. The volume of the solution was adjusted to obtain final Si/Al molar ratios of 40, 20, 10, 5 and 2.5. This mixture was then heated at 353 K for 1 h to ensure that the aluminum precipitated properly, where the mixture was previously diluted with H_2O until it reached pH 3.7. Next, it was left to cool at room temperature and solid SBA-15 was added. The temperature was then increased again to 353 K and held constant for 3 h. Finally, the solid was filtered, dried and calcined at 873 K for 4 h (heating rate of 1 K min^{-1}).

To provide the catalysts a hydrogenation function, a non-noble metal, such as cobalt, was selected for the catalytic process. Thus, the different Al-modified SBA-15 supports with variable amounts of aluminum were impregnated with an aqueous solution of $Co(NO_3)_2{\cdot}6H_2O$ salt. The incipient wet volume of SBA-15 was 3 mL of H_2O per g support and, accordingly, a cobalt nitrate solution to obtain a Co metallic concentration of 10 wt% was prepared. Finally, the impregnated solid was dried at 393 K for 12 h and calcined at 773 K for 5 h in an oven (heating ramp 1.5 K min^{-1}). These calcined samples were activated by H_2 reduction before measuring their catalytic activity, as will be explained in more detail below. The acid supports and catalysts were labeled as SBA-*x*Al and CoSBA-*x*Al, where *x* refers to the nominal Si/Al molar ratio.

2.2. Techniques of characterization

The chemical analysis of the calcined catalysts was performed with inductively coupled plasma atomic emission spectroscopy (ICP-AES) using a Perkin-Elmer Optima 3300 DV instrument. Prior to the analysis, the samples were solubilized in a mixture of HF, HCl, HNO_3 and H_3PO_4 and homogenized in a high-pressure microwave oven (Multiwave 3000 Anton Paar) for 2 h. The resulting solutions were diluted to 50 mL using Milli-Q deionized water.

The textural parameters were evaluated from nitrogen adsorption–desorption isotherms at 77 K, as determined using an automatic ASAP 2020 system from Micromeritics. Prior to the measurements, the samples were outgassed at 473 K and 10^{-4} mbar overnight. The surface areas were determined by using the Brunauer–Emmett–Teller (BET) equation, assuming a cross section of 16.2 $Å^2$ for the nitrogen molecule. The pore size distribution, the average pore diameter (D_p), and the total pore volume (V_p) were calculated from the isotherm desorption branch using the non-local density functional theory.

The TPR profiles were registered using a semiautomatic Micromeritics TPD/TPR 2900 apparatus. Before the reduction experiment, the calcined sample (*ca.* 80 mg loaded in a U-shaped reactor) was heated at 393 K under a He flow (35 mL min^{-1}) for 45 min to remove the physically adsorbed H_2O. After the sample cooled to room temperature, the TPR profile was recorded by heating the sample from 323 K to 973 K in an Ar/H_2 flow (48 mL min^{-1}, 10 vol% H_2) at a heating rate of 10 K min^{-1}. The water formed in the reduction reaction was trapped by passing the exit flow through a cold trap immersed in a liquid N_2/isopropyl alcohol bath (193 K).

X-ray photoelectron spectra (XPS) were collected using a Physical Electronics PHI 5700 spectrometer with non-monochromatic Al Kα radiation (300 W, 15 kV, and 1486.6 eV) with a multichannel detector. The spectra of the samples were recorded in the constant pass energy mode at 29.35 eV using a 720 mm diameter analysis area. Charge referencing was measured against adventitious carbon (C 1s at 284.8 eV). The Co 3d, Al 2p, Si 2p, C 1s and O 1s regions were scanned a sufficient number of times to obtain high signal-to-noise ratios. A PHI ACCESS ESCA-V6.0F software package was used for acquisition and data analysis. A Shirley-type background was subtracted from the signals. The recorded spectra were always fit using Gaussian–Lorentzian curves to determine the binding energies of the different element core levels more accurately. Reduced catalysts were stored in sealed vials in an inert solvent (cyclohexane). The sample preparation was performed in a dry box under a N_2 flow, where the solvent was evaporated before its introduction into the analysis chamber and directly analyzed without any previous treatment.

Aluminum coordination was evaluated by ^{27}Al MAS NMR spectra recorded with a Bruker AV-400 (9.4 T) spectrometer (Rheinstetten, Germany) using a BL-4 probe with zirconia rotors. The spectra were obtained using a spinning speed of ν_R = 10 kHz, a pulse width of 1 μs (corresponding to π/12 rad pulse length), a relaxation delay of 1 s, and typically 1200 scans.

The total acidity was measured using temperature-programmed desorption of ammonia (NH_3-TPD). The *in situ* reduced catalysts (0.1 g) were pretreated at 773 K for 1 h and then cooled to 373 K under a 50 mL min^{-1} Ar flow to remove the adsorbed surface species. Then, a flow of 5 vol% NH_3/He at 50 mL min^{-1} was passed through the sample bed for 1 h at 373 K, and subsequent flushing with an Ar flow at the same temperature was used to remove the physisorbed ammonia. The NH_3 desorption was performed from 373 to 1073 K at a heating rate of 10 K min^{-1}. The TPD analyses were registered using a Balzer Prisma™ quadrupole mass spectrometer (QMS 200) following the fragments m/z = 16 (NH_2^+), m/z = 17 (NH_3^+ and H_2O^+), m/z = 18 (H_2O^+), m/z = 28 (N_2^+ and CO^+), m/z = 30 (NO^+), m/z = 40 (Ar^+), m/z = 44 (N_2O^+), and m/z = 46 (NO_2^+) to follow the desorption of ammonia and to discard the oxidation of NH_3 to nitrogen oxides. The quantitative analysis of the desorbed ammonia was based on the m/z = 16 signal by integrating the area under this desorption curve. Previous calibration of this signal was properly conducted by passing streams with different NH_3 concentrations.

Diffuse reflectance infrared Fourier transform (DRIFT) spectra were collected with a Nicolet 5700 spectrometer equipped with a Hg–Cd–Te cryodetector with high sensitivity and working in the spectral range of 4000–650 cm^{-1}. A diffuse reflectance accessory (Praying Mantis-Harrick Co) was used as an optical mirror accessory. Approximately 30 mg of previously ground samples were placed in a high-temperature catalytic reaction chamber (HVC-DRP Harrick Scientific Products, NY) that allows treatment *in situ* at high temperatures. Before introducing the probe molecule, the solid sample was pretreated with a flow of 20% (v/v) O_2/Ar while being heated at 573 K, which was then left for 1 h to clean the surface of the supports or catalysts. In the case of catalysts containing cobalt, reduction under a 10% H_2/Ar flow at 723 K for 1 h was conducted. Afterward, the temperature was decreased to 298 K under an Ar flow; once at 298 K, the Ar was circulated across a bubbler with deuterated acetonitrile for 10 min. The fraction of physically or more weakly adsorbed CD_3CN was removed by flushing the reaction chamber with Ar (bypassing the bubbler). The DRIFT spectra of the deuterated acetonitrile were recorded at 128 scans with a resolution of 4 cm^{-1} at different temperatures and times during flushing with Ar.

2.3. Activity measurements

Fixed-bed continuous-flow catalytic studies were conducted in a 1/4″ tubular stainless-steel reactor at 523 K with 3 MPa H_2 controlled by a back-pressure regulator. The catalyst (0.25 g) was loaded between two end plugs of quartz wool. Prior to the reaction, the catalyst was reduced with an H_2 flow (50 mL min^{-1}) at 773 K with a heating rate of 2 K min^{-1} until the temperature reached 573 K. Once this temperature was reached, the heating ramp was changed to 1 K min^{-1} until it reached 773 K, where it was held for 10 h. Finally, it was cooled to the reaction temperature (523 K). Then, 10 wt% LA/ethanol solution was pumped into the reactor at different contact times, and the H_2 flow was adjusted to 20 mL min^{-1}. Although a liquid LA/ethanol solution is fed to the reactor, under the actual reaction conditions, the simulation with Advanced System for Process Engineering (ASPEN) software indicated that the reaction in the catalyst bed takes place in the gas phase, which is desired to avoid leaching of the cobalt and coke formation, which may have a lesser impact on deactivation during long-term continuous experiments. Downstream of the catalyst bed zone, at room temperature, the reaction mixture goes back to the liquid phase.

The product samples were analyzed in a gas chromatograph (Shimadzu GS2010) equipped with an SHRXI-5MS capillary column (30 m × 0.25 mm × 0.25 μm) and a flame ionization detector. Before the GC analysis, the samples were prepared by adding cyclohexanol (*ca.* 0.1 g) as an internal standard to an aliquot of the reaction products. LA conversion is defined as the ratio between the outlet molar flow of LA consumed in the reaction to the molar flow of LA initially fed in the reactor. The yield is defined as the ratio of the amount of molar flow of the product formed to the total molar flow of LA initially present. The selectivity is defined as the result of dividing the yield value by the LA conversion. The identification of different products was conducted in a GC-MS (Shimadzu QP2010S) equipped with an SHRXI-5MS capillary column as well.

3. Results and discussion

3.1. Characterization of the CoSBA-*x*Al catalysts

Table 1 compiles the experimental chemical analysis data of the calcined catalysts using inductively coupled plasma atomic emission spectroscopy (ICP-AES) technique. The empirical content of Co is quite close to the theoretical nominal value (10 wt%) for all samples. However, in terms of the Al content, its actual incorporation is lower than intended, which is more evident for samples with a higher aluminum content (a lower Si/Al ratio), indicating that part of the Al used in the preparation was not incorporated in the precursor. In any case, the empirical and nominal aluminum content follows the same trend: the Al concentration in each sample is roughly doubled in successive samples of the series. Therefore, these catalysts are suitable for conducting a study on the role of the Al content or surface acidity of these bifunctional catalysts on the catalytic properties.

The N_2 adsorption/desorption isotherms of the calcined CoSBA-*x*Al catalysts exhibit a type IV isotherm with an H2 hysteresis loop (Fig. S1a in the ESI†). The presence of a pore filling step with a narrow range of P/P_0, along with its

Table 1 Chemical analysis (ICP-AES) and textural properties of the CoSBA-*x*Al catalysts

	ICP-AES		N_2 isothermal (textural properties)				
Catalysts	Co (%)	Si/Al	S_{BET} ($m^2\ g^{-1}$)	t_{plot} ($m^2\ g^{-1}$)	V_{pore} ($cm^3\ g^{-1}$)	V_{mic} ($cm^3\ g^{-1}$)	D_{pore} (nm)
CoSBA	10.3	∞	392	123	0.340	0.028	4.8
CoSBA-40Al	10.2	47.6	325	118	0.295	0.048	4.4
CoSBA-20Al	9.7	24.5	293	86	0.281	0.035	4.3
CoSBA-10Al	9.4	12.2	196	26	0.212	0.009	4.6
CoSBA-5Al	9.7	7.5	183	29	0.191	0.011	4.4
CoSBA-2.5Al	9.6	5.2	139	17	0.160	0.005	4.4

reversibility, is consistent with the presence of mesoporous with highly ordered cylindrical pores of uniform size interconnected by intrawall micropores.[19,20] In terms of the surface area, Table 1 collects the S_{BET} associated with the total porosity of the samples, where the area associated exclusively to micropores, which was determined by method *t*, has also been compiled. In both cases, an increase in the aluminum content in the series results in a decrease in the surface area. This same trend is determined for the pore volume. In terms of the mesopore size distribution, no significant differences are observed throughout the series (see the last column on Table 1 and Fig. S1b†). It can be concluded that although the incorporation of aluminum and cobalt on SBA-15 decreases its surface area and pore volume, it does not significantly affect the structural properties of the starting SBA-15, as confirmed by small-angle powder XRD analysis (see Fig. S2†). All these results indicate that pores are blocked *via* incorporation of oxide species.[21]

To study the effect of the aluminum content on the reducibility of cobalt species, hydrogen temperature-programmed reduction (H_2-TPR) experiments were conducted. The Co_3O_4 spinel phase was the only Co crystalline phase identified by X-ray powder diffraction (see Fig. S3†) in the calcined CoSBA-*x*Al samples. Fig. 1 shows the TPR profiles of the calcined CoSBA-*x*Al samples. The Al-free CoSBA sample displays two peaks in the range of 500–700 K, with maxima at 580 and 609 K. These two reduction peaks are widely accepted to be associated with the two reduction steps of the Co_3O_4 spinel phase, first to the CoO phase and then to metallic cobalt (Co_3O_4 → CoO → Co^0). These two reduction processes have also been described for the Co_3O_4 phase supported on SBA-15.[11,21,22] For the Al-containing samples, these two reduction peaks are also observed in this same range of temperatures. In general, a slight shift to lower temperatures in both reduction peaks was observed for the samples with aluminum contents up to that of the CoSBA-10Al sample, specifically at 546 and 584 K. In contrast, for the samples with higher aluminum contents (CoSBA-5Al and CoSBA-2.5Al) these peaks shift to higher temperatures (at exactly 597 and 632 K).

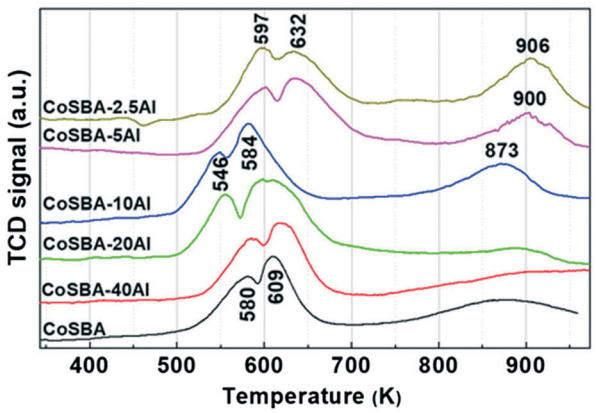

Fig. 1 TPR profiles of different calcined CoSBA-*x*Al samples.

It is known that cobalt dispersion, heterogeneity in particle size and support texture can modify the TPR profile.[23] It should be mentioned that these peaks are asymmetrical and challenging to fit into a single peak, suggesting that each of them is the result of two or more contributions. Thus, the reduction temperature is often directly related to the dispersion of the cobalt oxide species and the strength of its interaction with the support. Therefore, these data suggest that at low or moderate aluminum contents, the reducibility of the cobalt spinel is slightly favored by the presence of aluminum, while for a high aluminum content, the reducibility is more complicated, possibly because the interaction between the cobalt spinel and the support increased as the Al concentration increased.

Moreover, an additional reduction peak emerges in the temperature range of 850–975 K in the CoSBA-10Al, CoSBA-5Al and CoSBA-2.5Al samples, but this peak is incipient in the rest of the samples. Since this third reduction peak cannot be associated with cobalt aluminate ($CoAl_2O_4$) species, which require much higher temperatures of above 1073 K,[24] this peak can be better attributed to the reduction of another mixed phase of cobalt–aluminum oxide, nonstoichiometric aluminate.[25,26] After observing the reduction profiles of the calcined samples, the activation temperature of 773 K was chosen to reduce the most easily reducible species of cobalt; it was assumed that after this activation, only the Co^{2+} species that interact strongly with the support remain, which are mainly present in the samples with higher aluminum contents. Activating the samples at a temperature higher than 773 K to reduce all the Co^{2+} to Co^0 could imply the destruction of the mesoporous structure of the support. In summary, the TPR experiments show that incorporating Al affects the reducibility of the supported Co species.

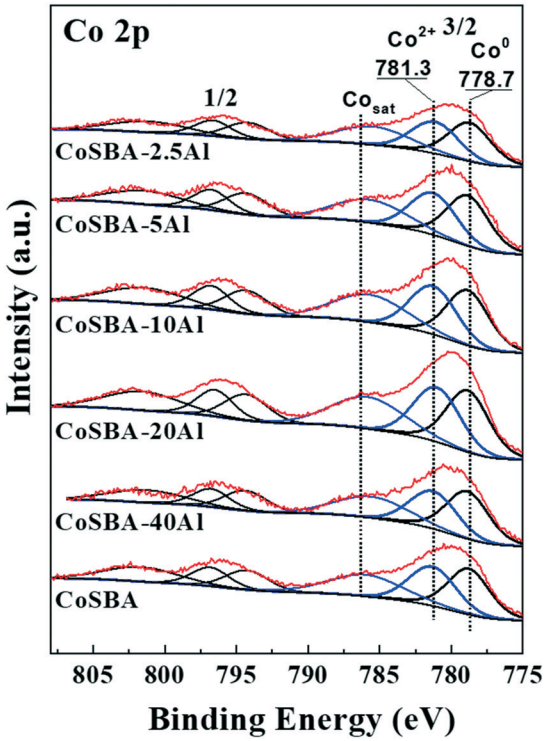

Fig. 2 XPS spectra of Co 2p core level for the CoSBA-*x*Al catalysts.

The oxidation state and chemical composition on the surface of the catalysts were analyzed *via* X-ray photoelectronic spectroscopy (XPS). Previous to this analysis, the samples were reduced following the same activation procedure performed in the reactor (up to a temperature of 773 K under H_2 with a flow rate of 50 mL min^{-1} for 10 h). Fig. 2 shows the XPS spectra of the Co 2p level, but we will only pay attention to the Co $2p_{3/2}$ component. The BE values are located at *ca.* 778.7 and 781.3 eV and assigned to the Co^0 and Co^{2+} ion species, respectively, whereas a third weak peak at *ca.* 786 eV represents the shake-up peak (Co_{sat}) due to the presence of cobalt ions.[27,28] Si 2p, Al 2p and O 1s core levels exhibit BE values expected for these mesoporous materials; the values are compiled in Table 2. According to the TPR results, after the reduction process at 773 K, Co^{2+} ions were only expected in the three catalysts with the highest aluminum contents, which showed a third species of cobalt that was reducible at temperatures above 850 K. However, Co^{2+} ions are observed on the surface of all catalysts in the series. The presence of Co^{2+} species can also be explained by the transferring of the samples from the reactor where the reduction is conducted to the XPS chamber. It may have resulted in the oxidation of the outermost layer of some of the metallic Co particles driven by the unavoidable contact with traces of ambient air. This could be the reason why the Co^{2+}/Co^0 ratio is similar for all samples.

Table 2 also shows that the Si/Al atomic ratio on the surface decreased as the aluminum content increased, which agrees with the bulk values determined by chemical analysis (see Table 1). Moreover, the Co/(Si + Al) atomic ratio derived from the XPS analysis was used as an indication of the dispersion of cobalt species on the surface; with some limitations this ratio has also been used previously for Co supported catalysts.[28–30] This atomic ratio increases with the aluminum content, indicating that the dispersion of Co is favored by the presence of aluminum (even though the incorporation of Al causes a decrease in the surface area). This increase in the dispersion of Co species is an evidence of the influence of Al oxide on Co oxide and strongly suggests the existence of an interaction between the cobalt and aluminum oxide species.[30] Summarizing, the XPS results evidence that incorporating Al favors the dispersion of the Co species.

The coordination of Al atoms in the catalysts was evaluated by ^{27}Al MAS NMR. The spectra of the catalysts after the incorporation of cobalt are similar (see, for example, CoSBA-20Al in comparison to SBA-20Al), and therefore the information extracted for the Al coordination by this technique is valid for both the supports and the catalysts. The spectra of the SBA-*x*Al supports are shown in Fig. 3. In general, the samples present two contributions: a peak at δ = 53 ppm ascribed to the framework aluminum species in tetrahedral coordination (Al^{IV}), and peaks at δ ranging from 0 to 6 ppm assigned to the extra-framework aluminum species in octahedral coordination (Al^{VI}).[19,31] When the Al content is low (Si/Al >10), the tetrahedral Al sites predominate and only a few species of octahedral Al are observed. For samples with

Table 2 Characterization data of the CoSBA-*x*Al catalysts

Catalyst	Binding energies (eV) and atomic ratios by XPS						NH_3-TPD μmol g^{-1}
	Al 2p	Si 2p	O 1s	Co $3p_{3/2}$	Si/Al	Co/Si + Al	
CoSBA		103.5	532.7(95%) 529.8 (5%)	778.7(53%) 781.3(47%)		0.197	29
CoSBA-40Al	74.7	103.6	532.8(89%) 530.2(11%)	778.5(56%) 781.4(44%)	73.60	0.223	73
CoSBA-20Al	74.8	103.1	532.5(91%) 529.7 (9%)	778.8(54%) 781.0(46%)	23.44	0.259	167
CoSBA-10Al	75.0	103.3	532.5(93%) 529.7 (7%)	778.8(52%) 781.3(48%)	14.14	0.255	262
CoSBA-5Al	74.9	103.2	532.4(88%) 529.8(12%)	778.8(54%) 781.2(46%)	6.78	0.267	382
CoSBA-2.5Al	75.0	103.2	532.5(85%) 530.1(15%)	778.7(55%) 781.1(45%)	3.99	0.299	436

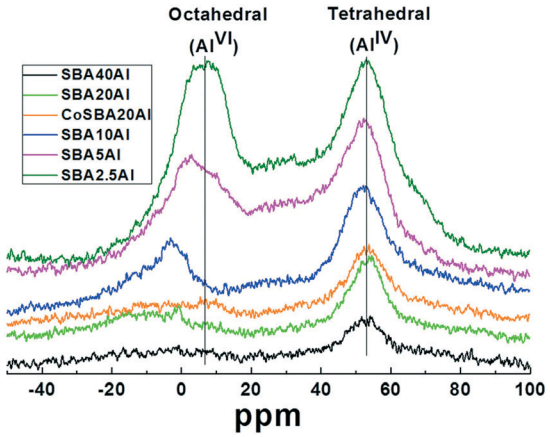

Fig. 3 ^{27}Al MAS NMR spectra of the SBA-*x*Al supports.

higher Al concentrations (Si/Al ≤10), although the concentration of tetrahedral sites increases, there is a faster relative increase in the concentration of octahedral sites, whose presence in the SBA-2.5Al sample is as significant as that of the tetrahedral sites. Therefore, at low aluminum contents, Al is predominantly incorporated into the SBA framework as tetrahedral Al, but when the aluminum content increases, the SBA framework is no longer capable of incorporating successive amounts of Al and extra-framework octahedral Al appears. Consequently, for Si/Al <20, the number of tetrahedral sites remains quite constant, whereas the concentration of octahedral (extra-framework) Al sites increases. The presence of distorted tetrahedral or five-coordinated aluminum cannot be disregarded due to the low-intensity signal observed at approximately 30 ppm.[32] In summary, although the number of Al sites increases, the ratio of Al_{tetra}/Al_{octa} decreases with the decrease in the Si/Al ratio, indicating that samples with lower Al content possess the largest relative percentage of Al incorporated in an SBA framework.

To evaluate the total amount and the strengths of the acid sites on the catalyst surface, temperature-programmed desorption of ammonia (NH_3-TPD) was performed for the reduced catalysts. Fig. 4 displays the desorption profiles of ammonia. A broad peak of desorption is observed between the 440 and 923 K interval. Two peaks can be clearly discerned at 580 and 673 K for the CoSBA-40Al and CoSBA-20Al samples, those with a lower aluminum content, whereas in the remaining samples the contribution peaking at 673 K is only observable as a shoulder of the main peak at 580 K. However, an exact assignment cannot be made since in these catalysts this broad and intense peak is the result of the contribution of acid centers of different nature and strength (as will be observed below) associated with the presence of aluminum ions in tetrahedral and octahedral coordination, Co^{2+} ions and silanol groups.

The total number of acid centers increases with the aluminum content. In terms of quantification, it is possible to calculate the total number of μmol of ammonia desorbed

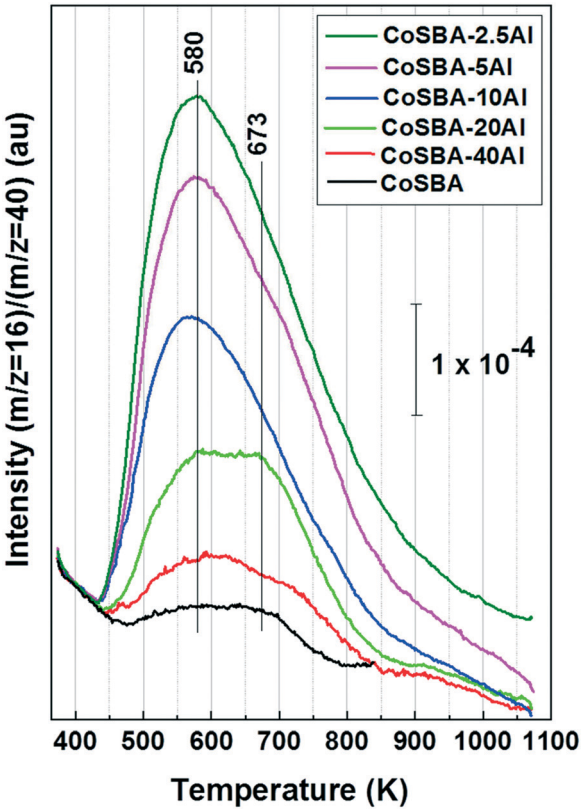

Fig. 4 NH_3-TPD profiles of the CoSBA-*x*Al catalysts.

per gram of catalyst. The values obtained are shown in last column of Table 2. The surface acidity of the samples is mainly associated with the presence of Al. As the Al content in the catalyst increases, the number of acid centers increases as well, although the proportion is not exactly linear. At higher aluminum contents, the surface acidity does not grow at the same rate as the Al content.

The Brønsted/Lewis nature and strength of the acid sites were also studied employing the diffuse reflectance infrared Fourier transform (DRIFT) technique using deuterated acetonitrile as the probe molecule. If CH_3CN is used the *ν*CN band is overshadowed by the Fermi resonance between the *ν*CN and the combination of $\delta_s(CH_3)$ + *ν*C–C frequencies. Therefore, the use of CD_3CN facilitates the assignment of infrared bands.[33,34] Moreover, the dynamic diameter of this molecule is small, so diffusion problems within the channels of SBA-15 are not expected. Acetonitrile chemisorbed on Lewis acid sites (LAS) displays a *ν*CN vibration distinguishable (>2300 cm^{-1}) from that assigned to acetonitrile chemisorbed on Brønsted acid sites (BAS, <2300 cm^{-1}).[35]

Fig. 5 shows the different infrared spectra of the supports and catalysts. Fig. 5A shows the spectra obtained for the various SBA-*x*Al supports after deuterated acetonitrile (CD_3-CN) adsorption and subsequent flushing with Ar at 373 K for 5 min. (see Fig. S4A and B† as examples of how the intensity of the bands in SBA-10Al and CoSBA-10Al samples, respectively, evolves during the entire process of CD_3CN

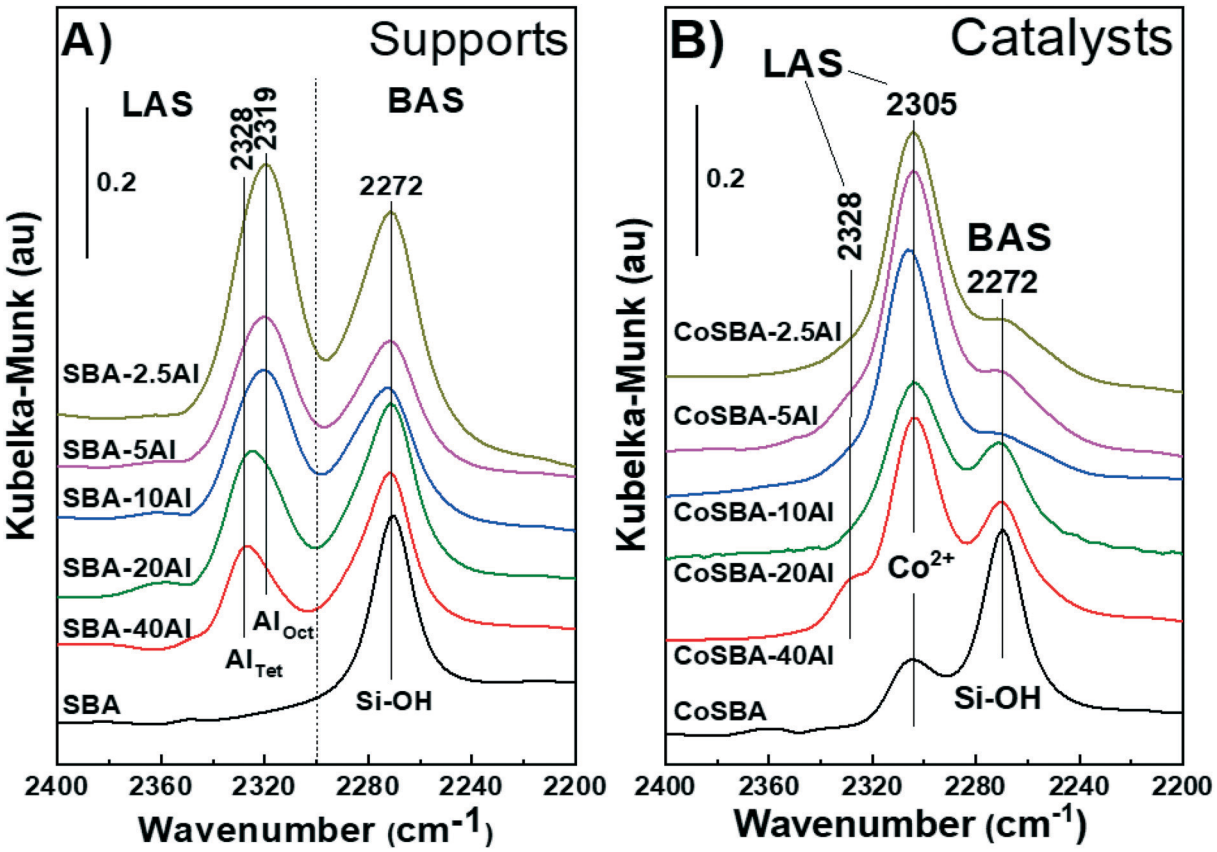

Fig. 5 DRIFT spectra after adsorption of deuterated acetonitrile of the CoSBA-*x*Al samples. (A) Supports and (B) reduced catalysts.

adsorption and subsequent Ar flushing at different temperatures and times). In Fig. 5A, two adsorption bands are shown. One is at 2272 cm^{-1}, which is associated with CD_3CN adsorption on the surface Brønsted acid sites (BAS), essentially due to silanol groups.[36,37] This assignation was confirmed by the fact that when the CD_3CN was outgassed by flushing at different temperatures and times, an increase in the intensity of the free silanol groups at 3740 cm^{-1} was also observed (this is not shown in the figure for the sake of simplicity). The second band has a maximum adsorption centered at 2328 cm^{-1}, which is associated with tetrahedral aluminum sites (SBA-40Al sample), centers responsible for high strength Lewis acid sites (LAS).[35–37] When this peak maximum was observed in more detail, a shift up to 2319 cm^{-1} was observed upon increasing the aluminum content, indicating the presence of a higher proportion of octahedral Al (SBA-2.5Al sample), as has been followed above by ^{27}Al NMR-MAS analysis. This shift is explained by the fact that the lower the frequency, the lower the acid strength of the acid centers. A displacement in the same direction has been described for LAS to coordinate tetrahedral and octahedral aluminum in zeolites.[35]

Fig. 5B shows the spectra obtained for the different calcined Co-containing SBA-*x*Al catalysts. The incorporation of cobalt drastically changes the surface acidity of the supports, though the bands associated with silanol groups (2272 cm^{-1}) and Al_{tet} (2328 cm^{-1}) are also observed. For catalysts with a lower aluminum content (CoSBA-40Al), the band at 2328 cm^{-1}, which represents the stronger Lewis acid sites associated with tetrahedral Al sites, is still clearly observed (in the rest of the samples, the latter band is observed as a shoulder of the main 2305 cm^{-1} peak). After incorporating cobalt, a prominent band at 2305 cm^{-1}, associated with weak LAS, is generated clearly in those catalysts containing Al. The wavenumber of the 2305 cm^{-1} band is considerably low to be associated with tetrahedral and octahedral aluminum for zeolites.[35] While an infrared band in the range 2310–2305 cm^{-1} has been previously associated with the presence of Co^{2+} ions supported on zeolites by several groups,[36,38] the fact that the appearance of this band is related to the vanishing of the Al_{oct} band at 2319 cm^{-1} suggests that Co^{2+} species are preferentially related to previously existing octahedral aluminum. Therefore, it can be concluded that aluminum oxide stabilizes the formation of weak LAS centers *via* the cobalt ions on the surface.[31,33] A similar effect has been observed for supported Cu/SiO_2 catalysts where the interaction of the oxide precursor with the support generates weak Lewis acid sites by the presence of surface Cu^{2+} ions.[39,40]

Summarizing, regarding the surface acidity of the catalysts, all the catalysts present weak BAS due to the presence of silanol groups. The incorporation of aluminum generates up to three types of LAS with different strengths.

Two types of strong or moderate LAS are due to the presence of Al in tetrahedral and octahedral coordination, respectively. In addition, extra-framework aluminum oxide induces the formation of another weak LAS center associated with Co^{2+} ions.

3.2. Catalytic activity

Fig. 6 shows the yield of the reaction products *versus* time on stream (TOS) for the different CoSBA-*x*Al catalysts; the applied weight-hourly space velocity (WHSV) is also

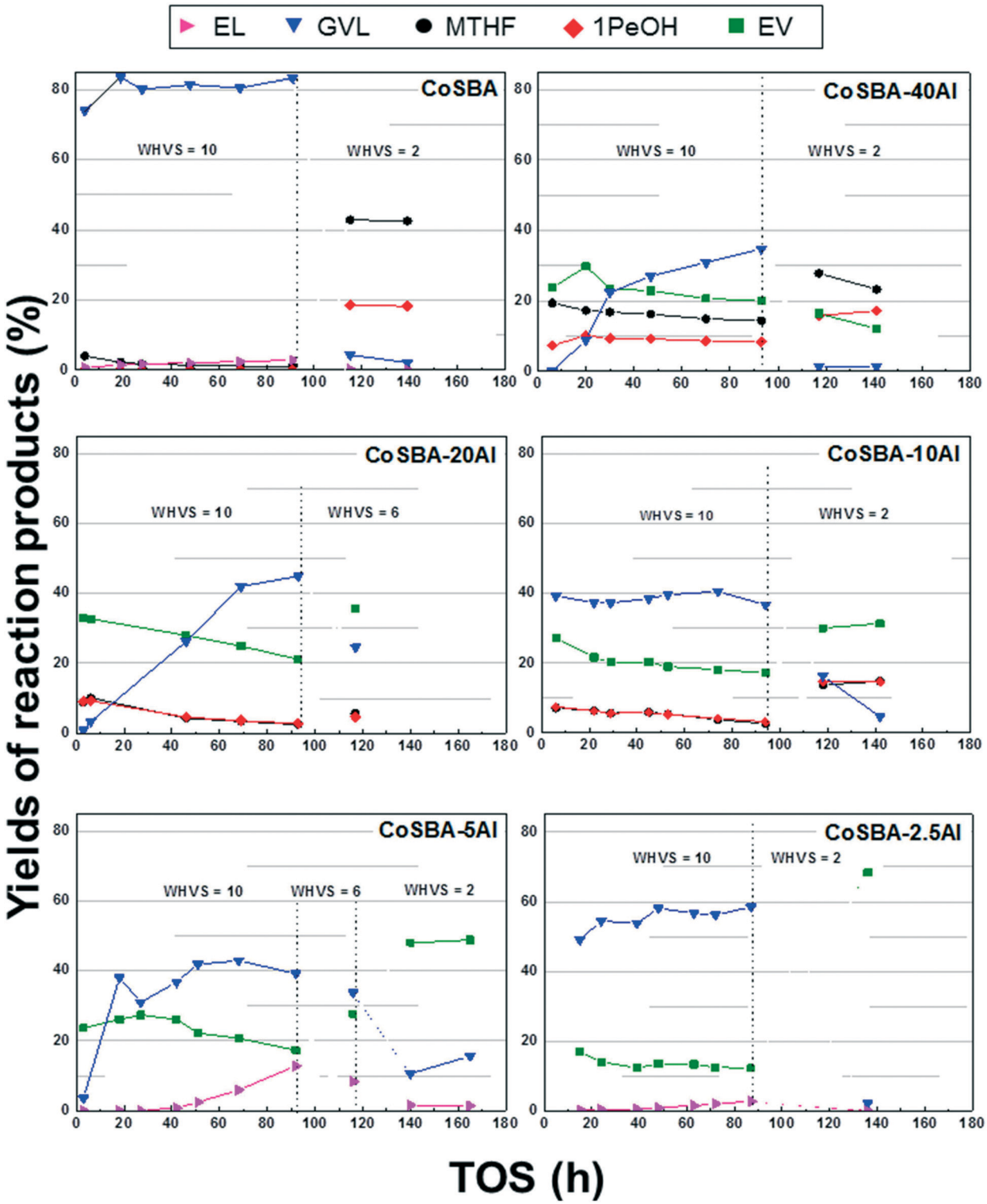

Fig. 6 Product yields *versus* time on stream (TOS) for the CoSBA-*x*Al catalysts. Reaction conditions: 10 wt% LA in ethanol, 0.25 g catalyst, 513 K and 3.0 MPa H_2.

indicated. The experimental procedures for all the catalysts were similar, starting the reaction at WHSV = 10 h^{-1} for approximately 90 h and then decreasing the WHSV by reducing the LA ethanol solution flow rate, which increases the contact time. The LA conversion is complete for all the catalysts of the series, and therefore it is not shown in the figure. The reaction product yields depend on the composition of the tested catalyst. The yields of the main products, such as ethyl levulinate (EL), gamma-valerolactone (GVL), methyl tetrahydrofuran (MTHF), 1-pentanol (1PeOH) and ethyl valerate (EV), are shown. However, other minor products, such as valeric acid (VA), pentenoic acid and ethyl pentenoate isomers, and ethyl pentyl ether (EPE), are also detected by GC-MS analysis, but with yields of less than 3%. In any case, the carbon balance did not close and therefore, other products that are not detected by gas chromatography can be formed during the reaction. It is well known that coke-like products can be formed when hydrotreating organic compounds at temperatures above 500 K in the presence of acidic sites[41,42] that can account, at least partially, for the lack of carbon balance. These carbonaceous coke-like residues can have their relevance in the deactivation by fouling the active centers in the catalyst, as will be mentioned below.

To facilitate the description of Fig. 6, the widely accepted LA catalytic hydrodeoxygenation reaction pathways[7,43] are presented in Fig. 7. Ethyl levulinate (EL) is the first product of the reaction and it can even be formed thermally under our reaction conditions; EL was identified as the main reaction product in a blank test using an inert bed (sieved quartz). GVL is the pivotal intermediate compound in this reaction. There are two competitive transformations of GVL, which will depend on the catalyst and, more specifically, on the balance between the reducing and acid centers on the surface of the catalyst.

GVL transformation can proceed (i) *via* a non-selective hydrogenation route on the reduction centers (metallic cobalt) to obtain mainly MTHF, 1PeOH and even ethyl pentyl ether (EPE); the latter can be formed after etherification on acid sites of 1PeOH with the ethanol solvent; and (ii) the selective route on acid centers with the ring opening of GVL occurring in the bond between the furan oxygen and the carbon with the methyl group, giving ethyl pentenoate (or pentenoic acid) isomers which can be subsequently reduced to obtain ethyl valerate (or valeric acid in aqueous medium).

As shown in Fig. 6, the Al-free catalyst (CoSBA), which hardly presents acidity, mainly forms GVL at WHSV = 10 h^{-1}. This indicates that the catalyst has sufficient reducing ability to allow for the hydrocyclisation of LA/EL to GVL (first step of the reaction). Moreover, this catalyst was considerably stable after 90 h under these reaction conditions. The modification of the space velocity to WHSV = 2 h^{-1} resulted in an evident change in the reaction of the GVL intermediate: GVL practically disappears and follows the so-called non-selective route, forming methyl tetrahydrofuran (MTHF) and 1-pentanol (1PeOH), which are identified and stable along the time on stream. This same reaction pathway, in the absence of surface acidity, has already been reported for the Co/SiO_2 catalyst.[43]

For the rest of the catalysts, which contain different proportions of aluminum on the support, the catalytic course of the reaction changes significantly. In the case of the CoSBA-40Al catalyst, the presence of acid sites *via* the incorporation of Al species on the support modifies the

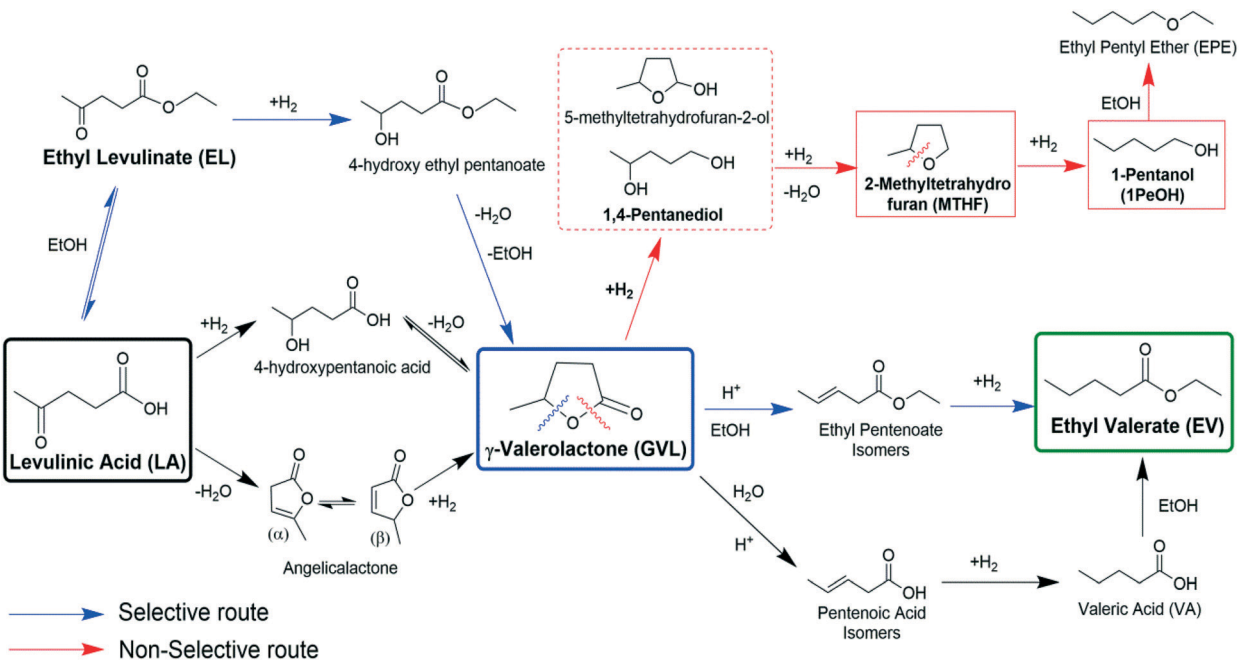

Fig. 7 Reaction pathways of levulinic acid (LA) transforming into ethyl valerate (EV). Adapted from Luo *et al.*[7]

behavior of the catalyst and favors the ring opening of GVL, yielding EV, whose yield is between 20% and 30% at WHSV = 10 h^{-1}. The GVL yield is initially considerably low, but after 30 h on stream, GVL becomes the major product without significantly affecting the EV yield. This transient behavior of GVL is not related to the dead volume effects of the reactor because the rest of the products remain quite constant along the experiment. It is clear that, regarding GVL formation, there is a conditioning period of the catalyst. MTHF and 1PeOH coming from the non-selective route of GVL are also obtained. Additionally, some amount of ethyl pentyl ether (EPE) has also been detected due to the etherification reaction between 1PeOH and the ethanol solvent. These findings suggest that the reducing capacity of this catalyst is higher than for the CoSBA catalyst *via* the presence of aluminum. The presence of acid sites at the surface of the support modifies the reducibility and dispersion of Co species due to a possible interaction between both metals,[44] which can enhance the hydrogenating characteristics of the cobalt particles and the promotion of the non-selective hydrogenation route. Similarly to the previous free aluminum catalyst, when the WHSV was decreased to 2 h^{-1}, GVL disappears by transformation *via* non-selective paths (formation of MTHF and 1PeOH and other non-detected products), which also decreases the EV yield.

Next, the behavior of the CoSBA-20Al catalyst is discussed. At WHSV = 10 h^{-1}, the catalytic performance is quite similar to that of the CoSBA-40Al system, with an initial transient behavior for GVL formation, becoming the most important product after some time on stream, and the formation of EV and other products such as MTHF and 1PeOH. The latter two products have lower yields than in the CoSBA-40Al case. In both CoSBA-20Al and the next catalyst of the series, CoSBA-10Al, the yield values for MTHF and 1PeOH are similar and therefore the two lines overlap. At longer contact times (WHSV = 2 h^{-1}), the GVL yield decreases at the expense of the formation of more EV. Lower amounts of MTHF and 1PeOH are also formed. In the CoSBA-10Al catalyst, no transient behavior is observed for GVL, and no EPE was detected.

Concerning the series of catalysts with higher Al contents, it is expected that the existence of a higher proportion of acid sites will provide greater importance to the selective GVL ring-opening route. Thus, the CoSBA-5Al catalyst essentially leads to GVL, EV when setting the conditions for longer contact times (moving from WHSV = 10 h^{-1} to 6 h^{-1}), while the products of the non-selective route are not detected. When WHSV was further reduced to 6 h^{-1} and 2 h^{-1} (longer contact times), the EV yield increases due to the enhanced transformation of intermediate products, such as EL and GVL into EV, which is now promoted by the larger concentration of acid sites. A similar behavior is also observed for the CoSBA-2.5Al catalyst (see Fig. 6); actually, a higher yield of EV was observed at WHSV = 2 h^{-1}, close to 70%, which is the largest yield of all the catalyst series. EV is essentially the unique product identified under these conditions.

All the above results can be discussed in the context of the critical question: the fate of the GVL intermediate when the aluminum oxide is incorporated into the support and how it evolves when increasing the aluminum content. At a WHVS of 10 h^{-1}, for the aluminum-free catalyst (CoSBA), the reaction only gives GVL: GVL conversion is not allowed under our operating conditions. However, when catalysts with low and moderate aluminum contents (CoSBA-40Al, CoSBA-20Al and CoSBA-10Al) are tested, the GVL reaction progresses *via* both competitive routes. Then, GVL can be partially transformed *via* the non-selective way to give MTHF and 1PeOH, and simultaneously another fraction of GVL is converted to EV by the selective route. Therefore, the presence of aluminum in the catalyst is critical to favor both routes. In our opinion, the particular pathway to give EV is promoted by the presence of Al due to the acidity that it directly provides to the catalyst by the presence of tetrahedral and octahedral Al sites, and indirectly provides by the stabilization of cobalt ions after the incorporation of aluminum.

To complete the picture, it is necessary to analyze the reaction when the WHVS is decreased to 2 h^{-1}. The contact time is then longer and the reaction can proceed further. For the catalyst without aluminum, CoSBA, the catalyst can now convert GVL to MTHF and 1PeOH (non-selective route). The catalysts with low or moderate amounts of aluminum (CoSBA-40Al, CoSBA-20Al and CoSBA-10Al) can conduct the two GVL conversion routes. Finally, in catalysts with a higher aluminum content (CoSBA-5Al and CoSBA-2.5Al) that already gave the selective route at high WHVS (low contact time), now at WHSV = 2 h^{-1} selectively transforms GVL to EV.

Summarizing, these bifunctional CoSBA-*x*Al catalysts are active and selective in the cascade conversion of LA to EV in ethanol. GVL is the main reaction intermediate, which is formed, and then two competitive reactions, the non-selective GVL route to MTHF and 1PeOH and the selective GVL ring-opening route to EV, occur. Which route predominates will depend on the concentration of the acid site on the surface on the catalyst and the contact time selected. All these results essentially agree with the mechanism already proposed in the literature. We will discuss next the relevance of Lewis acid sites in the cascade reaction.

3.3. Role of the surface acidity on the catalytic properties

First, it should be mentioned that the incorporation of aluminum in the support, in addition to providing acidity to the support, affects the reducibility and dispersion of the surface species of cobalt. In the catalysts with a higher proportion of aluminum, the stabilization of Co^{2+} ions is clearly observed. This means that as the aluminum content in the support increases, the hydrogenating capacity decreases. The relative proportion of metallic species of Co is lower. This is an advantage for catalysts with high Al content since a high hydrogenating capacity favors the conversion of LA to undesirable products (MTHF and 1PeOH).

On the other hand, it is known that the acid centers are required in different stages of the cascade reaction to transform LA to EV[4] and that the rate-determining step is the GVL ring-opening reaction.[14] Therefore this function gains greater relevance within the context of our CoSBA-*x*Al systems. It should be remembered that these bifunctional catalysts do not present strong BAS. Only considerably weak silanol groups are observed and are in practice quite inactive in the ring-opening reaction, as can be deduced from the negligible selectivity to EV when using the CoSBA catalyst. This catalyst has mainly silanol groups. According to our results, under our operating conditions (gas phase), the LAS must catalyze this reaction. In this CoSBA-*x*Al system, we have reported three LAS types of different strengths: tetrahedral and octahedral Al^{3+} and Co^{2+} ions. Their different acid strengths, and therefore their intrinsic activity in the acid-driven reactions, together with their relative concentration in the catalysts, explains the catalytic behavior of the catalysts studied in this work. The acid strength of the three LAS centers identified in our catalysts follows the trend $Al_{tet} > Al_{oct} > Co^{2+}$. The tetrahedral Al predominates at low Al content. When more Al is incorporated, both Al_{tet} and Al_{oct} become more concentrated but Al_{oct} concentration grows faster and practically outweighs the Al_{tet} concentration in the CoSBA-2.5Al. A weaker acidity corresponds to its lower intrinsic activity in the GVL ring-opening reaction. With the increasing of Al content, a higher fraction of Co^{2+} species, resistant to reduction, is stabilized on the surface of the activated catalyst. According to the results presented in this article, these weak LAS are also selective for the ring-opening reaction of the GVL. These weak LAS acid centers are capable of opening the ring of GVL; their less intrinsic activity is compensated for by the higher concentration of these centers. Recently, Velisoju *et al.*[45] have described the formation of Ni^{2+}/Ni^0 in Ni/ZSM5 catalysts promoted by the incorporation of Mo. They suggested that the Ni^{2+} species stabilized by interaction with Mo can perform the GVL opening ring by cracking the C–O bond on the methyl group side of the GVL molecule. Although these authors have used γ-valerolactone instead of levulinic acid as the substrate, these findings support our results since there is an explicit parallelism between the presence of Ni^{2+} species described by them and the stabilized Co^{2+} species described in our catalysts, especially in supports with high Al content.

In summary, although it is not surprising that the incorporation of Al provides LAS in our bifunctional catalysts, the catalytic results indicate that these LAS are active in the direct reaction from LA to EV. It must also be stressed that even the weak LAS centers associated with Co^{2+} ions are active and considerably selective under our reaction conditions. These weak LAS reach the highest concentration in the sample with the highest Al content, which is quite selective to EV, the product of interest.

To further evaluate the intrinsic activity of the acid centers and their deactivation, Fig. 8 shows the rate of EV formation per gram of CoSBA-*x*Al catalysts for WHSV = 10 and 2. This allows us to properly evaluate the possible deactivation of the different catalysts. We have conducted the reaction under

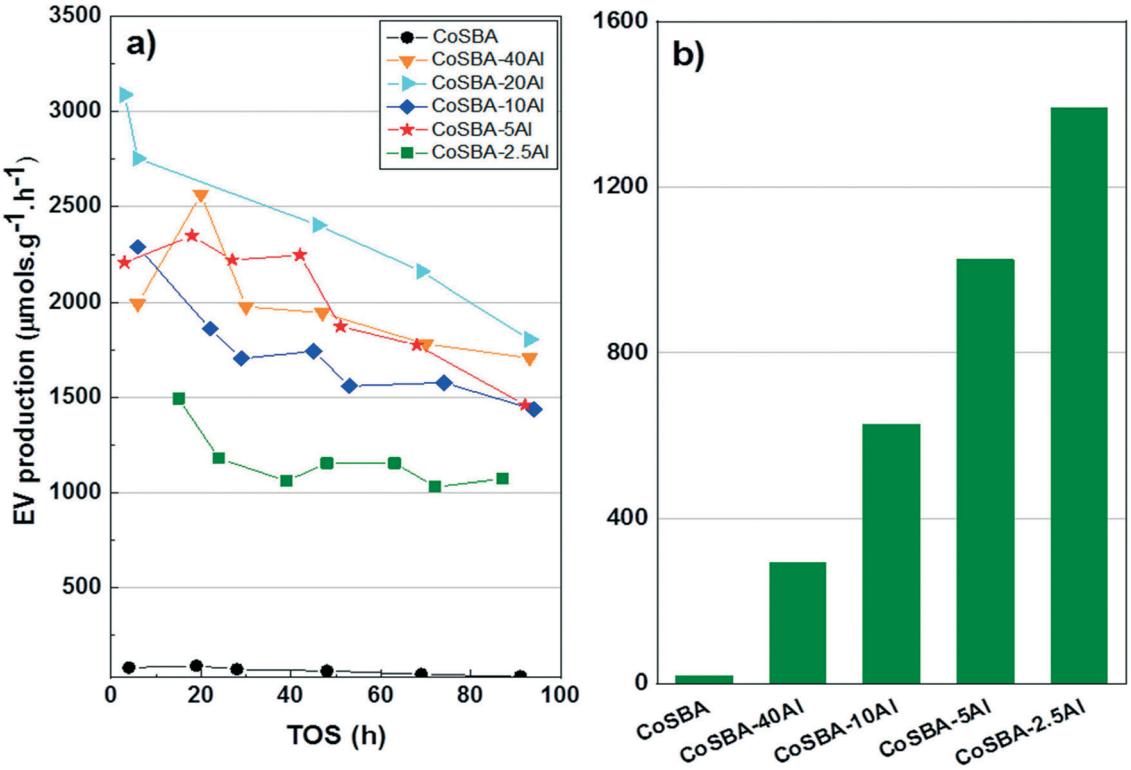

Fig. 8 EV productivity for the different CoSBA-*x*Al catalysts under the following conditions: (a) WHSV = 10 h^{-1} and (b) WHVS = 2 h^{-1}.

WHSV = 10 h^{-1} to detect the slow deactivation processes (see Fig. 8a), where the production of EV is displayed against the TOS. All the bifunctional catalysts present a slight deactivation with time on stream. The observed trend is that the higher the aluminum concentration, the more stable the catalyst is, although the productivity and yield of EV are lower. If we take into account that the aluminum concentration approximately doubles in two consecutive samples of the series, it can be deduced that the intrinsic activity in EV of the LAS associated with Al_{tet} (predominant in the first samples of the series) is higher than that of Al_{oct} and Co^{2+} that are proportionally in greater quantity in the samples of the series with more aluminum content.

In the case of WHSV = 2 h^{-1} (see Fig. 8b where the values have been derived from the average value when there is more than one point in these conditions), it is observed that the higher the concentration of aluminum in the catalyst, the higher the productivity and yield of EV due to the higher surface concentration of acid centers, as found by the TPD of ammonia (see Fig. 4). For the CoSBA-2.5Al catalyst we have reported an EV productivity of 1391 μmol g^{-1} h^{-1}, which is one of the highest values reported in the bibliography. This data has more value if we consider that it has been obtained after it has been subjected to a total of 140 h, at WHSV = 10 and 2 h^{-1} for around 90 and 50 hours, respectively, of reaction.

In general, samples with less Al initially produce more EV; but they are deactivated; the cascade of reactions is stopped in GVL and, consequently, less EV is formed. It seems that in samples with less Al, aluminum centers in tetrahedral and octahedral coordination (LAS) predominate, which are very active in the GVL ring-opening reaction but are also involved in the formation of coke deposits. The coke formation could explain the worse carbon balance in these samples. The fouling of the catalyst by the formed coke in practice decreases the number of acid centers exposed to the surface. In contrast, in samples with a high Al content, LAS Co^{2+} ions are also more concentrated. They are weaker and therefore less active in the GVL ring-opening reaction but the lower strength makes them even more stable because they are also less effective for coke production and less prone to fouling (deactivated).

In summary, the catalyst with the largest amount of aluminum (CoSBA-2.5Al) presents the highest EV yield. This performance is derived from the lower proportion of metallic Co species decreasing the hydrogenating capacity of this catalyst. This decrease is a positive result because it prevents GVL hydrogenation to undesired products. The Co^{2+} surface ions have been stabilized by incorporation of the aluminum into the support, modifying the reducibility and dispersion of cobalt species. The presence of LAS associated with these Co^{2+} species that, although with low intrinsic activity in the selective GVL ring-opening reaction, are highly concentrated in this sample and also possess less activity in the undesirable and deactivating formation of coke.

These results allow for expanding the possibilities of these bifunctional catalysts. It has been observed that both functions (hydrogenating and acidity) are modulated with the aluminum content present in the acid support. The selectivity and, consequently, the yield of the reaction products will depend on the reaction conditions, where the balance between the metallic centers and the amount and strength of the Lewis acid centers plays an essential role. Different cobalt contents and higher aluminum concentrations need to be explored for these systems. At this point, we have to mention that the micro or mesoporous nature of the support is also essential in the catalytic behavior along with the aluminum content, as has been previously reported.[9]

4. Conclusions

Bifunctional CoSBA-*x*Al catalysts are active for the direct conversion of levulinic acid to ethyl valerate in the gas phase using a solution of levulinic acid in ethanol in a continuous system. Once the intermediate product γ-valerolactone has been formed, it can follow two competitive routes: (i) non-selective, giving methyl tetrahydrofuran and 1-pentanol, and (ii) selective, giving ethyl valerate, for which the presence of Al is required. With an increase in the aluminum content in the series, a progressive conversion of γ-valerolactone towards the particular path to ethyl valerate is observed, to the detriment of the non-selective way.

The originality of this work is derived from these bifunctional CoSBA-*x*Al catalysts, except for the inactive weak silanol groups, which only present LAS that are active in the cascade reaction of levulinic acid to ethyl valerate, including determining the γ-valerolactone ring-opening step. Specifically, three types of Lewis acid sites are identified: tetrahedral and octahedral Al ions join with a fraction of non-reduced cobalt (Co^{2+} ions) stabilized by the incorporated Al in the support.

The best and most stable catalyst is the one with the highest concentration of aluminum (CoSBA-2.5Al), where an ethyl valerate yield of 70% is reached at longer contact times (WHSV = 2 h^{-1}). This behavior is due to the presence of a weaker, and consequently lower, intrinsic activity than Al ions, and higher density of acid centers associated with the presence of Co^{2+} ions, which are capable of selectively activating to give the corresponding ethyl pentenoate and allow for a subsequent reduction in ethyl valerate, avoiding its deactivation by coke fouling. Simultaneously, the higher Co^{2+}/Co^{0} ratio on the surface of this catalyst (see DRIFT spectra in Fig. 5B) decreases its hydrogenating capacity. It prevents the hydrogenation reactions of the γ-valerolactone intermediate, giving undesired products, such as methyl tetrahydrofuran and 1-pentanol, and increasing the ethyl valerate yield instead. This catalyst also showed promising stability in a 140 h on-stream run.

Conflicts of interest

There are no conflicts to declare.

Acknowledgements

Financial support from the Spanish Ministry of Economy and Competitiveness (RTI2018-94918-B-C41/C43) is gratefully acknowledged. R. M. also thanks the Ministry of Education, Culture and Sports for a "Salvador de Madariaga" grant (PRX16/00167) and the Fulbright Commission in Spain for co-financing his stay at UW-Madison.

References

1 F. D. Pileidis and M. M. Titirici, *ChemSusChem*, 2016, **9**, 562–582.
2 Z. Xue, Q. Liu, J. Wang and T. Mu, *Green Chem.*, 2018, **20**, 4391–4408.
3 J. P. Lange, R. Price, P. M. Ayoub, J. Louis, L. Petrus, L. Clarke and H. Gosselink, *Angew. Chem., Int. Ed.*, 2010, **49**, 4479–4483.
4 Z. Yu, X. Lu, J. Xiong and N. Ji, *ChemSusChem*, 2019, **12**, 3915–3930.
5 K. Kon, W. Onodera and K. I. Shimizu, *Catal. Sci. Technol.*, 2014, **4**, 3227–3234.
6 X. M. Gu, B. Zhang, H. J. Liang, H. Bin Ge, H. M. Yang and Y. Qin, *Ranliao Huaxue Xuebao*, 2017, **45**, 714–722.
7 W. Luo, P. C. A. Bruijnincx and B. M. Weckhuysen, *J. Catal.*, 2014, **320**, 33–41.
8 T. Pan, J. Deng, Q. Xu, Y. Xu, Q. X. Guo and Y. Fu, *Green Chem.*, 2013, **15**, 2967–2974.
9 M. Muñoz-Olasagasti, A. Sañudo-Mena, J. A. Cecilia, M. López Granados, P. Maireles-Torres and R. Mariscal, *Top. Catal.*, 2019, **62**, 579–588.
10 Z. Yi, D. Hu, H. Xu, Z. Wu, M. Zhang and K. Yan, *Fuel*, 2020, **259**, 3–6.
11 M. Audemar, C. Ciotonea, K. De Oliveira Vigier, S. Royer, A. Ungureanu, B. Dragoi, E. Dumitriu and F. Jérôme, *ChemSusChem*, 2015, **8**, 1885–1891.
12 P. Sun, G. Gao, Z. Zhao, C. Xia and F. Li, *ACS Catal.*, 2014, **4**, 4136–4142.
13 N. Karanwal, D. Verma, P. Butolia, S. M. Kim and J. Kim, *Green Chem.*, 2020, **22**, 766–787.
14 W. Luo, U. Deka, A. M. Beale, E. R. H. Van Eck, P. C. A. Bruijnincx and B. M. Weckhuysen, *J. Catal.*, 2013, **301**, 175–186.
15 P. Sun, G. Gao, Z. Zhao, C. Xia and F. Li, *Appl. Catal., B*, 2016, **189**, 19–25.
16 J. Zhou, R. Zhu, J. Deng and Y. Fu, *Green Chem.*, 2018, **20**, 3974–3980.
17 C. E. Chan-Thaw, M. Marelli, R. Psaro, N. Ravasio and F. Zaccheria, *RSC Adv.*, 2013, **3**, 1302–1306.
18 S. Liu, G. Fan, L. Yang and F. Li, *Appl. Catal., A*, 2017, **543**, 180–188.
19 M. Gómez-Cazalilla, J. M. Mérida-Robles, A. Gurbani, E. Rodríguez-Castellón and A. Jiménez-López, *J. Solid State Chem.*, 2007, **180**, 1130–1140.
20 R. Zhang, D. Shi, N. Liu, Y. Cao and B. Chen, *Appl. Catal., B*, 2014, **146**, 79–93.
21 M. Kondeboina, S. S. Enumula, V. R. B. Gurram, R. R. Chada, D. R. Burri and S. R. R. Kamaraju, *J. Ind. Eng. Chem.*, 2018, **61**, 227–235.
22 Y. Yang, G. Lv, L. Deng, B. Lu, J. Li, J. Zhang, J. Shi and S. Du, *Microporous Mesoporous Mater.*, 2017, **250**, 47–54.
23 B. Ernst, A. Bensaddik, L. Hilaire, P. Chaumette and A. Kiennemann, *Catal. Today*, 1998, **39**, 329–341.
24 W. J. Wang and Y. W. Chen, *Appl. Catal.*, 1991, **77**, 223–233.
25 G. Jacobs, T. K. Das, Y. Zhang, J. Li, G. Racoillet and B. H. Davis, *Appl. Catal., A*, 2002, **233**, 263–281.
26 P. Arnoldy and J. A. Moulijn, *J. Catal.*, 1985, **93**, 38–54.
27 H. Zhou, J. Song, H. Fan, B. Zhang, Y. Yang, J. Hu, Q. Zhu and B. Han, *Green Chem.*, 2014, **16**, 3870–3875.
28 A. Boix, E. E. Miró, E. A. Lombardo, M. A. Bañares, R. Mariscal and J. L. G. Fierro, *J. Catal.*, 2003, **217**, 186–194.
29 R. Balzer, L. F. D. Probst, V. Drago, W. H. Schreiner and H. V. Fajardo, *Braz. J. Chem. Eng.*, 2014, **31**, 757–769.
30 A. Y. Khodakov, W. Chu and P. Fongarland, *Chem. Rev.*, 2007, **107**, 1692–1744.
31 S. Chen, J. Li, Y. Zhang, Y. Zhao and J. Hong, *Catal. Sci. Technol.*, 2013, **3**, 1063–1068.
32 T. H. Chen, B. H. Wouters and P. J. Grobet, *Eur. J. Inorg. Chem.*, 2000, 281–285.
33 S. Jolly, J. Saussey and J. C. Lavalley, *J. Mol. Catal.*, 1994, **86**, 401–421.
34 R. Mariscal, M. López-Granados, J. L. G. Fierro, J. L. Sotelo, C. Martos and R. Van Grieken, *Langmuir*, 2000, **16**, 9460–9467.
35 A. G. Pelmenschikov, R. A. Van Santen, J. Jänchen and E. Meijer, *J. Phys. Chem.*, 1993, **97**, 11071–11074.
36 J. Chen, J. M. Thomas and G. Sankar, *J. Chem. Soc., Faraday Trans.*, 1994, **90**, 3455–3459.
37 M. Paniagua, G. Morales, J. A. Melero, J. Iglesias, C. López-Aguado, N. Vidal, R. Mariscal, M. López-Granados and I. Martínez-Salazar, *Catal. Today*, 2020, **367**, 228–238.
38 O. Bortnovsky, Z. Sobalík and B. Wichterlová, *Microporous Mesoporous Mater.*, 2001, **46**, 265–275.
39 N. Scotti, M. Dangate, A. Gervasini, C. Evangelisti, N. Ravasio and F. Zaccheria, *ACS Catal.*, 2014, **4**, 2818–2826.
40 F. Zaccheria, N. Scotti, M. Marelli, R. Psaro and N. Ravasio, *Dalton Trans.*, 2013, **42**, 1319–1328.
41 D. M. Bibby, R. F. Howe and G. D. McLellan, *Appl. Catal., A*, 1992, **93**, 1–34.
42 I. Van Zandvoort, Y. Wang, C. B. Rasrendra, E. R. H. Van Eck, P. C. A. Bruijnincx, H. J. Heeres and B. M. Weckhuysen, *ChemSusChem*, 2013, **6**, 1745–1758.
43 G. Novodárszki, H. E. Solt, J. Valyon, F. Lónyi, J. Hancsók, D. Deka, R. Tuba and M. R. Mihályi, *Catal. Sci. Technol.*, 2019, **9**, 2291–2304.
44 R. Munirathinam, D. Pham Minh and A. Nzihou, *Ind. Eng. Chem. Res.*, 2018, **57**, 16137–16161.
45 V. K. Velisoju, D. Jampaiah, N. Gutta, U. Bentrup, A. Brückner, S. K. Bhargava and V. Akula, *ChemCatChem*, 2020, **12**, 1341–1349.